

Delineation of Hypoxia in Canine Myocardium Using PET and Copper(II)-Diacetyl-*bis*(*N*⁴-Methylthiosemicarbazone)

Jason S. Lewis, PhD¹; Pilar Herrero, MS¹; Terry L. Sharp¹; John A. Engelbach¹; Yasuhisa Fujibayashi, PhD, DMedSci²; Richard Laforest, PhD¹; Attila Kovacs, MD¹; Robert J. Gropler, MD¹; and Michael J. Welch, PhD¹

¹Division of Radiological Sciences, Mallinckrodt Institute of Radiology, Washington University School of Medicine, St. Louis, Missouri; and ²Biomedical Imaging Research Center, Fukui Medical University, Matsuoka, Fukui, Japan

Copper(II)-diacetyl-*bis*(*N*⁴-methylthiosemicarbazone) (copper-ATSM) is a hypoxia-avid tracer for the selective identification of hypoxic tissue. Using canine models of hypoxic myocardium, we report our findings on ⁶⁴Cu-ATSM PET (⁶⁴Cu is defined as either ⁶⁰Cu, ⁶¹Cu, or ⁶⁴Cu) for the delineation of ischemic and hypoxic myocardium. **Methods:** In protocol I, myocardial hypoxia was induced by global hypoxia (*n* = 3). In protocol II, myocardial ischemia was generated by occlusion of the left anterior descending coronary artery (*n* = 9). In protocol III, coronary artery stenosis was induced by a stenosis in the left anterior descending coronary artery (*n* = 4). PET dynamic data were acquired immediately after tracer injection. Tracer retention kinetics were analyzed using either monoexponential analysis ($1/k_{\text{mono}}$) or a simple 2-compartment model ($1/k_4$). **Results:** In protocol I, tracer retention in hypoxic myocardium was 2-fold greater than in normal myocardium, despite a 7-fold increase in blood flow (normal, $0.70 \pm 0.42 \text{ mL}\cdot\text{min}^{-1}\cdot\text{g}^{-1}$; hypoxic, $4.94 \pm 3.00 \text{ mL}\cdot\text{min}^{-1}\cdot\text{g}^{-1}$ [$P < 0.005$]). In protocol II, ~3 h after occlusion, retention of ⁶⁴Cu-ATSM within 20 min was greater in ischemic regions (myocardial blood flow, $0.28 \pm 0.26 \text{ mL}\cdot\text{min}^{-1}\cdot\text{g}^{-1}$) than in normal tissue (myocardial blood flow, $0.52 \pm 0.19 \text{ mL}\cdot\text{min}^{-1}\cdot\text{g}^{-1}$) ($1/k_{\text{mono}}$, $40.72 \pm 39.0 \text{ min}$ vs. $26.69 \pm 22.29 \text{ min}$ [$P < 0.05$]; $1/k_4$, $6.85 \pm 4.90 \text{ min}$ vs. $3.51 \pm 1.97 \text{ min}$ [$P < 0.05$]). In selected dogs, tracer retention decreased at 24 h, suggesting the development of necrosis with no subsequent retention of ⁶⁴Cu-ATSM. In protocol III, dobutamine infusion after stenosis placement resulted in increased tracer retention consistent with hypoxia in the damaged regions. **Conclusion:** ⁶⁴Cu-ATSM PET has shown quantitative selective uptake in hypoxic myocardium within 20 min of tracer administration in 3 canine models of hypoxia.

Key Words: copper(II)-diacetyl-*bis*(*N*⁴-methylthiosemicarbazone); imaging; ischemia; hypoxia

J Nucl Med 2002; 43:1557–1569

The primacy of myocardial ischemia, and resultant tissue hypoxia, in the pathophysiology of coronary artery disease is well established. Currently, all noninvasive approaches to detect myocardial ischemia measure either the level of myocardial oxygen supply or the downstream effects of myocardial hypoxia such as altered mechanical function or electric instability.

The importance of developing imaging agents capable of delineating hypoxia in tissue is well established (1,2). Misonidazole analogs and 2-nitroimidazole functionalities have been labeled with iodine radionuclides (e.g., ¹²³I-io-dozomycin arabinoside (3,4)) and with ^{99m}Tc for SPECT and ¹⁸F for PET imaging of hypoxia. The ^{99m}Tc-compounds ^{99m}Tc-HL91 (5), BMS-181321 (6), and BMS-194796 (7) have demonstrated increased uptake in hypoxic and low-flow ischemic myocardium. The PET agent ¹⁸F-fluoromisonidazole (FMISO) is retained in hypoxic tissue in the myocardium, and clinical studies show differences that can be imaged between normal and hypoxic tissues (8–11). Nitroimidazole-based agents suffer from 2 disadvantages, low cellular uptake and slow normal-tissue clearance, requiring long periods between injection and imaging (2,8,9).

Copper(II)-diacetyl-*bis*(*N*⁴-methylthiosemicarbazone) (copper-ATSM) is in a class of copper *bis*(thiosemicarbazones) that have been evaluated in vitro and display uptake that either is not hypoxia selective (e.g., copper[II]-pyruvaldehyde-*bis*(*N*⁴-methylthiosemicarbazone), copper-PTSM (12,13)) or is hypoxia selective (14–16). In vivo, ⁶⁴Cu-ATSM is rapidly retained in hypoxic tumors and myocardium but diffuses in normoxic tissue (14,17–19). In experimental tumor models, the selective uptake of ⁶⁴Cu-ATSM depended on the partial pressure of oxygen (pO₂), and a direct correlation between tissue uptake of ⁶⁴Cu-ATSM and tissue pO₂ was observed, with significantly greater retention in hypoxic tissue (14,18). Studies using an acute myocardial infarction rat heart model, in which oxygen concentration can be controlled, showed that specific retention of ⁶⁴Cu-ATSM is due to oxygen depletion (16). The results of preliminary studies in Japan have demonstrated the poten-

Received Feb. 25, 2002; revision accepted Jul. 9, 2002.
For correspondence or reprints contact: Michael J. Welch, PhD, Mallinckrodt Institute of Radiology, Washington University School of Medicine, Campus Box 8225, 510 S. Kingshighway Blvd., St. Louis, MO 63110.
E-mail: welchm@mir.wustl.edu

tial of ^{62}Cu -ATSM for hypoxia imaging in acute ischemia syndromes (19). Because of the increasing availability of positron-emitting isotopes of copper (^{60}Cu [half-life ($t_{1/2}$) = 0.40 h, β^+ = 93%, electron capture (EC) = 7%], ^{61}Cu [$t_{1/2}$ = 3.32 h, β^+ = 62%, EC = 40%], ^{62}Cu [$t_{1/2}$ = 0.16 h, β^+ = 98%, EC = 2%], and ^{64}Cu [$t_{1/2}$ = 12.7 h, β^+ = 17.4%, EC = 43%]) (20–22), we have continued to investigate $^*\text{Cu}$ -ATSM (where $^*\text{Cu}$ is defined as either ^{60}Cu , ^{61}Cu , or ^{64}Cu) as a noninvasive selective marker for myocardial hypoxia in canine models of ischemia before human evaluation.

Previous studies using rodent hypoxia models have established the hypoxia selectivity of $^*\text{Cu}$ -ATSM in vivo (14,17,18), and the current study was undertaken to determine the selectivity of $^*\text{Cu}$ -ATSM for myocardial models of hypoxia in canines before human trials. Protocol I was undertaken to determine the relationship between $^*\text{Cu}$ -ATSM retention/washout and myocardial blood flow (MBF). Protocol II was undertaken to elucidate the usefulness of $^*\text{Cu}$ -ATSM PET for acute ischemic syndromes such as myocardial infarction when flow is limited. This model was also used to demonstrate the kinetics of $^*\text{Cu}$ -ATSM in necrotic tissue. Protocol III was undertaken to show the imaging characteristics of $^*\text{Cu}$ -ATSM when ischemia is induced without a severe flow limitation (as is observed in an abnormal rest/stress echocardiogram), which is the most common clinical scenario in which myocardial hypoxia is documented. Hypoxia and ischemia are 2 different physiologic states, and this study was performed to examine the oxygen-deprived myocardial states of both hypoxia and ischemia.

MATERIALS AND METHODS

All chemicals, unless otherwise stated, were purchased from Aldrich Chemical Co., Inc. (Milwaukee, WI). All solutions were prepared using distilled deionized water (Milli-Q; >18 M Ω resistivity). Radioactive samples were counted on a γ -counter (model 8000; Beckman, Irvine, CA).

Radioisotope Production and Characteristics

^{64}Cu -, ^{61}Cu -, and ^{60}Cu -ATSM were prepared as previously described (20,21). At our institution, we can make these 3 copper radioisotopes on demand, and the choice of which isotope to use for a particular study was based on radioactive half-life to allow for repeated imaging sessions when required. To ensure a similar resolution between each isotope, the phantom of Derenzo et al. (23) for ^{64}Cu and ^{60}Cu was imaged on our ECAT 962 HR $^+$ scanner (Siemens, Knoxville, TN). The phantom consists of 10-cm cylindrical holes drilled into a clear plastic cylinder (23). The rods are arranged in a pielike pattern and have diameters of 2.5, 3, 3.5, 4, 5, and 6.25 mm. The phantom was filled with water containing a dilute amount of ^{60}Cu or ^{64}Cu with a concentration of 296 kBq/mL. The total volume of the phantom is 220 mL. Imaging was performed by acquiring static emission data for 1 h. Images were then reconstructed with filtered backprojection using a ramp filter at Nyquist frequency and a zoom of 2. A calculated attenuation correction was applied. The resulting pixel size was 0.24 cm. The

entire volume of data for 1 bed position was reconstructed and contained 63 slices of 128 \times 128 pixels. Data were corrected for scatter using the manufacturer-provided method. The random coincidences were removed using the delayed window technique.

Animal Protocol

Male mongrel dogs (20–25 kg) were purchased from Butler Farms USA, Inc. (Clyde, NY). All animal experiments were conducted in compliance with the Guidelines for the Care and Use of Research Animals established by the Animal Studies Committee at our institution. Dogs were premedicated with 1–1.5 mg/kg of morphine sulfate injection (King Pharmaceuticals, Bristol, TN). Anesthesia was induced by 12.5 mg/kg of 5% sodium thiopental solution and maintained by titrating the recommended doses of α -chloralose as needed. Each dog was hemodynamically monitored throughout the experiment. Percutaneous sheaths were placed in bilateral femoral arteries and veins for direct arterial blood pressure measurement; anesthesia maintenance; and fluid, drug, or radiopharmaceutical administration. The sheaths were kept in situ until euthanasia.

Protocol I: Induction of Myocardial Hypoxia by Generation of Global Hypoxia ($n = 3$). The dogs were administered a fractional concentration of oxygen in inspired gas of 100%, and ^{15}O -H $_2$ O PET and ^{60}Cu -ATSM PET were performed as described in Imaging Protocols and Data Collection. After the first ^{60}Cu -ATSM PET scan was complete, global hypoxia was induced by ventilating the dog on 90% N $_2$:10% O $_2$ (24), a mixture for which, at these pO $_2$ levels, hypoxemia leads to hypoxia. The measurement of blood oxygen levels throughout the study demonstrated arterial blood hypoxemia, suggesting global tissue hypoxia, and with the evident increase in blood flow and the external signs of cyanosis, the presence of hypoxic myocardium was expected. After the arterial pO $_2$ levels decreased to 35%–45% that of baseline (approximately 50 min), ^{15}O -H $_2$ O and ^{60}Cu -ATSM PET imaging was repeated.

Protocol II: Induction of Acute Myocardial Ischemia ($n = 9$). Acute coronary occlusion was created in the mid left anterior descending (LAD) coronary artery by placement of a 3- to 5-mm copper coil under fluoroscopic guidance in a closed-chest preparation as previously described (25). Fluoroscopic imaging was performed on a cardiovascular mobile digital C-arm (OEC series 9800; General Electric Medical Systems, Milwaukee, WI). Complete coronary occlusion was documented with coronary catheterization and was confirmed by typical electrocardiographic signs of ischemia, including ST elevation and ventricular arrhythmia. ^{15}O -H $_2$ O and ^{61}Cu -ATSM (or ^{60}Cu -ATSM) were administered within 3 h of coil placement, and PET scanning proceeded as described in Imaging Protocols and Data Collection.

After the 3-h scan, 4 dogs were maintained over 24 h to determine the selectivity of $^*\text{Cu}$ -ATSM between ischemic and necrotic myocardium. ^{15}O -H $_2$ O and ^{64}Cu -ATSM were administered for a second time 22–24 h after coil placement, and PET scanning proceeded as described in Imaging Protocols and Data Collection. After euthanasia, infarct size (percentage of the total left ventricle) was determined semiquantitatively using 1% 2,3,5-triphenyltetrazolium chloride (TTC) staining based on previous methods (26,27). The same heart slices were examined on an electronic autoradiography system (InstantImager; Packard Instrument Co., Meriden, CT). Heart slices were mounted and placed in the InstantImager to show the distribution of ^{64}Cu -ATSM.

Protocol III: Induction of Demand Ischemia ($n = 4$). Coronary artery stenosis was induced by the insertion of a Teflon (Dupont,

Wilmington, DE) stenosis into the mid LAD coronary artery under fluoroscopic guidance as described previously (28). Fluoroscopic imaging confirmed placement of the Teflon stenosis, with the formation of between 65% and 80% stenosis as determined by the standard software package supplied with the cardiovascular mobile digital C-arm. In protocol III, because of the nature of the experiment and the titration of dobutamine (DOB), the use of $^{15}\text{O}\text{-H}_2\text{O}$ would have extended the length of intervention (to allow for ^{15}O decay) and would have caused a delay between MBF determination and $^{60}\text{Cu}\text{-ATSM}$ PET. Therefore, in protocol III, myocardial perfusion was measured with radioactive microspheres by following previously reported methods (29). The first $^{60}\text{Cu}\text{-ATSM}$ scan (and concurrent microsphere administration) was performed within 1 h of stenosis placement under resting conditions as described in Imaging Protocols and Data Collection. On completion of the first scan, the animals were titrated with DOB from 0 to 40 $\mu\text{g}/\text{kg}/\text{min}$ for 30 min. Because of the difficulty in measuring regional pO_2 , echocardiography was used as a surrogate marker for the presence of ischemia. Wall motion decreases and diminished systolic function in the LAD region (LADR), consistent with ischemia, were seen on the echocardiograms. In this protocol, once the stress echocardiogram confirmed the presence of ischemia, a second dose of $^{60}\text{Cu}\text{-ATSM}$ (or of ^{61}Cu - or $^{64}\text{Cu}\text{-ATSM}$) (and microspheres) was administered and a second $^{60}\text{Cu}\text{-ATSM}$ PET study was performed.

Imaging Protocols and Data Collection

PET studies were conducted on the ECAT 962 HR⁺ scanner. After a transmission scan, myocardial perfusion for protocols I and II was determined by administering 666–925 MBq of $^{15}\text{O}\text{-H}_2\text{O}$ as an intravenous bolus and acquiring dynamic PET data for 5 min (5-s frames). In protocol III, myocardial perfusion was measured with ^{85}Sr (rest) and ^{46}Sc (with DOB) microspheres (15 μm in 0.01% Tween; NEN Life Science Products, Inc. Boston, MA). In all protocols, $^{60}\text{Cu}\text{-ATSM}$ (labeled with ^{60}Cu [44.4–388.5 MBq], ^{61}Cu [222.0–240.5 MBq], or ^{64}Cu [214.6–569.8 MBq]) was administered as a bolus injection, followed by the immediate collection of dynamic data until 45 min.

Image Analysis

Myocardial $^{15}\text{O}\text{-H}_2\text{O}$ and $^{60}\text{Cu}\text{-ATSM}$ dynamic images were reoriented to generate standard short-axis and horizontal and vertical long-axis views. To generate myocardial time–activity curves from the global hypoxia studies (protocol I), for which no differences in regional flow or hypoxia were expected, regions of interest encompassing the anterolateral wall (3–5 cm^3) were placed on 2 or 3 standard short-axis slices of a composite $^{60}\text{Cu}\text{-ATSM}$ image. Myocardial time–activity curves for the ischemic studies (protocols II and III), for which regional flow and hypoxia heterogeneity were expected, were generated from normally perfused and ischemic myocardium by placing 3 or 4 regions of interest on the normal myocardium and 2 or 3 LADRs. $^{15}\text{O}\text{-H}_2\text{O}$ myocardial and blood time–activity curves were used in conjunction with a validated kinetic model (30) to estimate MBF ($\text{mL}\cdot\text{min}^{-1}\cdot\text{g}^{-1}$). In protocols II and III, regions were defined as hypoperfused or normal on the basis of both the $^{15}\text{O}\text{-H}_2\text{O}$ PET images and the $^{60}\text{Cu}\text{-ATSM}$ PET images. Anteroapical regions with activity less than 50% of peak radioactive counts were defined as hypoperfused. Regions representing myocardium remote from the LAD and with activity at 80%–100% of peak radioactive counts were defined as normally perfused. The same regions were then placed

on the $^{15}\text{O}\text{-H}_2\text{O}$ and $^{60}\text{Cu}\text{-ATSM}$ dynamic images to measure MBF (protocol II) and myocardial ischemia (protocols II and III), respectively.

Monoexponential Analysis. For each myocardial region generated from the $^{60}\text{Cu}\text{-ATSM}$ PET images, the washout phase (from the peak radioactive counts to the end of data collection) of the myocardial $^{60}\text{Cu}\text{-ATSM}$ curves was fitted to a simple monoexponential, and the estimated rate of clearance (k_{mono} [min^{-1}]) was assumed to be inversely proportional to $^{60}\text{Cu}\text{-ATSM}$ myocardial retention and, therefore, an index of myocardial hypoxia. The assumption that the washout phase is proportional to hypoxia is supported by results from experimental rodent tumor and ischemic myocardium models (17,18). Myocardial retention was then expressed as the inverse of k_{mono} (retention = $1/k_{\text{mono}}$ [min]). The k_{mono} values were obtained from the individual regions of interest and were averaged for the normally perfused regions (NLRs) and LADRs. Paired *t* tests were performed to determine statistical significance among grouped data. Correlations were calculated by linear regression.

Kinetic Modeling. A 2-compartment model (Fig. 1) was used to describe the myocardial kinetics of $^{60}\text{Cu}\text{-ATSM}$. This was a feasibility kinetic model, and full validation is required before routine use. Compartment 1 represents vascular $^{60}\text{Cu}\text{-ATSM}$ that exchanges with the extravascular and interstitial spaces, and compartment 2 represents $^{60}\text{Cu}\text{-ATSM}$ that enters the myocyte. Vascular $^{60}\text{Cu}\text{-ATSM}$ ($\text{Ca}[t]$) enters compartment 1 at a rate of K_1 ($\text{mL}\cdot\text{min}^{-1}\cdot\text{g}^{-1}$). Once the tracer is in this compartment, either it can diffuse back into the vasculature at a rate of k_2 (min^{-1}) or it can enter the myocyte (compartment 2) at a rate of k_3 (min^{-1}). Under normoxic conditions, $^{60}\text{Cu}\text{-ATSM}$ washes out of the cell at a rate of k_4 (min^{-1}), whereas under hypoxic conditions, copper-ATSM is selectively retained by the myocyte (i.e., decreased k_4). After correction of blood time–activity curves for $^{60}\text{Cu}\text{-ATSM}$ metabolites (to obtain the true input function), myocardial curves were used in conjunction with the input function to estimate model transfer rates K_1 – k_4 and the blood-to-tissue spillover fraction. The rate k_4 should, at that point, represent washout of tracer from the myocyte (and not from the entire myocardium, as k_{mono} does). For dogs in which perfusion was measured with $^{15}\text{O}\text{-H}_2\text{O}$, the tissue recovery coefficient obtained from $^{15}\text{O}\text{-H}_2\text{O}$ analysis was used to correct $^{60}\text{Cu}\text{-ATSM}$ counts (partial volume). For dogs in which radioactive microspheres were used instead of $^{15}\text{O}\text{-H}_2\text{O}$ PET, an average tissue recovery fraction obtained from the other studies was used. Myocyte tracer retention was then expressed as the inverse k_4 (retention $k_4 = 1/k_4$ [min]). The k_4 values were obtained from the individual regions of interest and were averaged for the NLRs and LADRs. Paired *t* tests were performed to determine

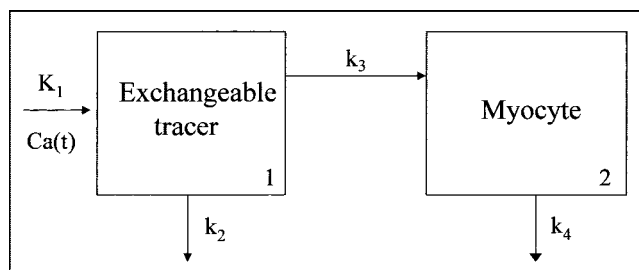


FIGURE 1. Two-compartment model used to model biokinetics of $^{60}\text{Cu}\text{-ATSM}$ in myocardium.

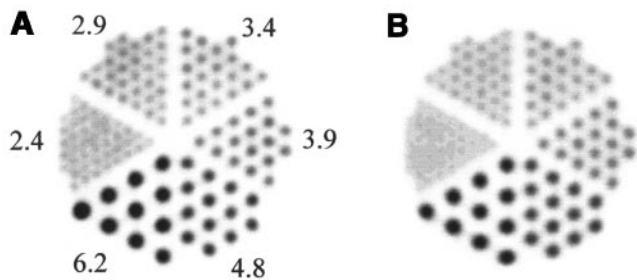


FIGURE 2. Phantom of Derenzo et al. (23) for ^{64}Cu (A) and ^{60}Cu (B). Unfavorable emissions associated with decay of ^{60}Cu have not reduced image quality in comparison with ^{64}Cu phantom in ECAT 962 HR⁺ scanner. Values shown are bore sizes, in millimeters.

statistical significance among grouped data. Correlations were calculated by linear regression.

Correction of Blood Activity for ^{64}Cu -ATSM Metabolites

To correct the input function (for kinetic modeling) obtained from PET images for the presence of ^{64}Cu -ATSM metabolites, the following procedure was performed on the basis of methods used in canine studies with the flow tracer copper(II)-pyruvaldehyde

bis(N_4 -thiosemicarbazone) (29). A bolus of 37 MBq of ^{64}Cu -ATSM was injected intravenously into 3 dogs. Sequential 500- μL arterial samples were withdrawn every 10 s for the first minute and every minute thereafter for 15 min. Triplicate 100- μL samples of the withdrawn blood were immediately added to 1 mL of 75% octanol. The tubes were rapidly stirred and centrifuged at 14,000 rpm for 5 min. The supernatant was aspirated, and the supernatant and pellet were counted in a γ -counter. Analysis by radio-TLC confirmed that extractable radioactivity was in the form of ^{64}Cu -ATSM. At each time point, the value of the fraction of octanol-extractable ^{64}Cu -ATSM in blood was obtained. The resulting curve represented the fraction of ^{64}Cu -ATSM present in the blood over time. A multiexponential function was fitted to this fraction so that it could be defined at any given time and used to correct the total blood activity of radiocopper obtained from the PET images. This function (with averaged parameter values) was used for all animals studied.

RESULTS

Isotope Imaging Characteristics

Shown in Figure 2 is the phantom of Derenzo et al. (23) for ^{64}Cu and ^{60}Cu . For both isotopes, all rod diameters can

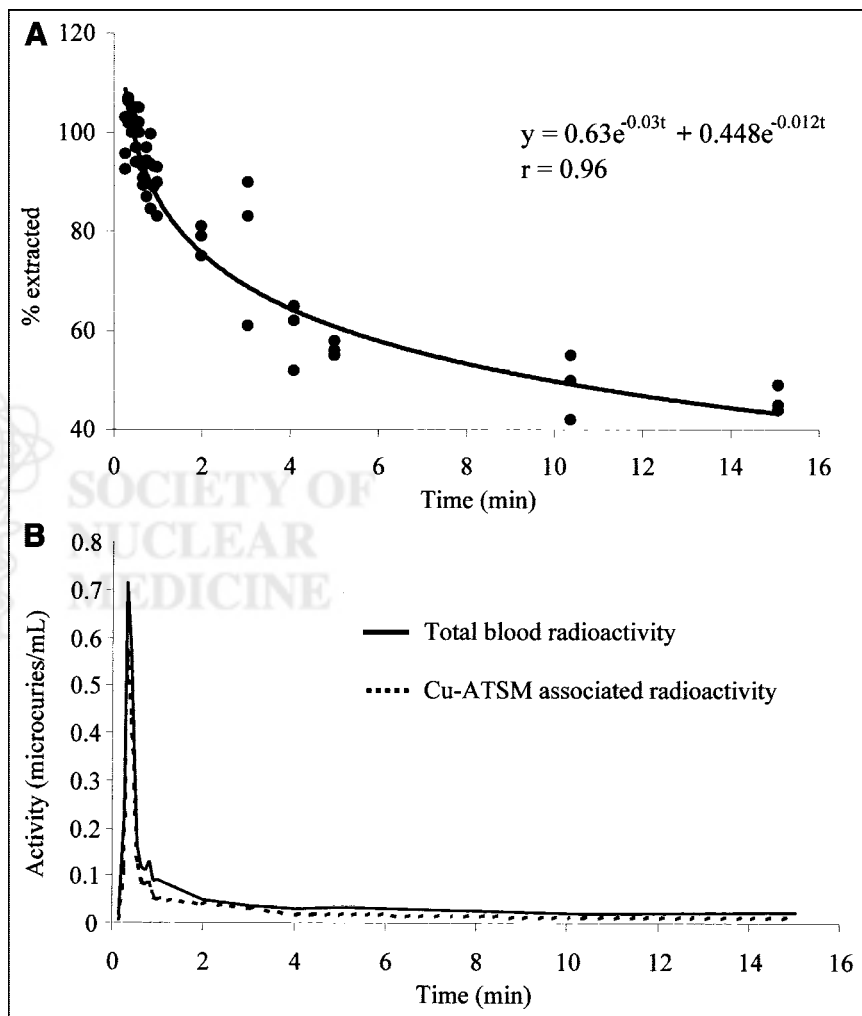


FIGURE 3. Time-activity curves generated from direct arterial sampling after arterial administration of 37 MBq of ^{64}Cu -ATSM to generate input function ($n = 3$ dogs). (A) Plot shows percentage of octanol-extractable ^{64}Cu -ATSM with respect to total ^{64}Cu -ATSM blood activity as function of time. (B) Plot shows total amount of radioactivity in arterial blood after injection of ^{64}Cu -ATSM as function of time and amount of radioactivity in form of ^{64}Cu -ATSM.

TABLE 1
 MBF Determined by $^{15}\text{O}\text{-H}_2\text{O}$ PET and $^*\text{Cu}\text{-ATSM}$ Retention as Shown by Monoexponential Analysis ($1/k_{\text{mono}}$) and Kinetic Modeling ($1/k_4$) for Protocol I

Dog no.	Baseline flow ($\text{mL} \cdot \text{min}^{-1} \cdot \text{g}^{-1}$)	Hypoxic flow ($\text{mL} \cdot \text{min}^{-1} \cdot \text{g}^{-1}$)	Flow ratio	Mean retention			
				Baseline		Hypoxic tissue	
				$1/k_{\text{mono}}$ (min)	$1/k_4$ (min)	$1/k_{\text{mono}}$ (min)	$1/k_4$ (min)
1	1.18 ± 0.06	8.39 ± 0.32	7.09	10.75 ± 0.46	2.84 ± 0.83	>100	18.35 ± 8.62
2	0.42 ± 0.04	2.99 ± 0.09	7.12	15.70 ± 1.23	2.63 ± 1.11	36.63 ± 19.05	4.11 ± 1.53
3	0.51 ± 0.02	3.43 ± 0.39	6.78	17.39 ± 0.21	8.70 ± 2.48	27.62 ± 13.74	34.48 ± 4.52
Mean \pm SD	0.70 ± 0.42	$4.94 \pm 3.00^*$	7.00 ± 0.19	14.61 ± 3.45	4.72 ± 3.44	54.75 ± 39.45	19.98 ± 15.19

* $P < 0.0001$ hypoxia vs. baseline.

be identified with the exception of the smallest rods when imaged with ^{60}Cu .

Correction of Blood Activity for Metabolites

Figure 3A shows the measured percentage of octanol-extractable $^{64}\text{Cu}\text{-ATSM}$ in blood with respect to total radioactivity as a function of time, and Figure 3B shows the total amount of radioactivity in arterial blood with respect to

time. It clearly demonstrates, for $^*\text{Cu}\text{-ATSM}$ activity, rapid extraction of radioactivity from the blood; the total radioactivity averaged approximately 13% of peak at 1 min and dropped to less than 0.5% at 5 min. When corrected for the octanol-extractable activity, the $^*\text{Cu}\text{-ATSM}$ blood activity is even lower at these times. It is hoped that generation of a similar correction will be clinically applicable to all sub-

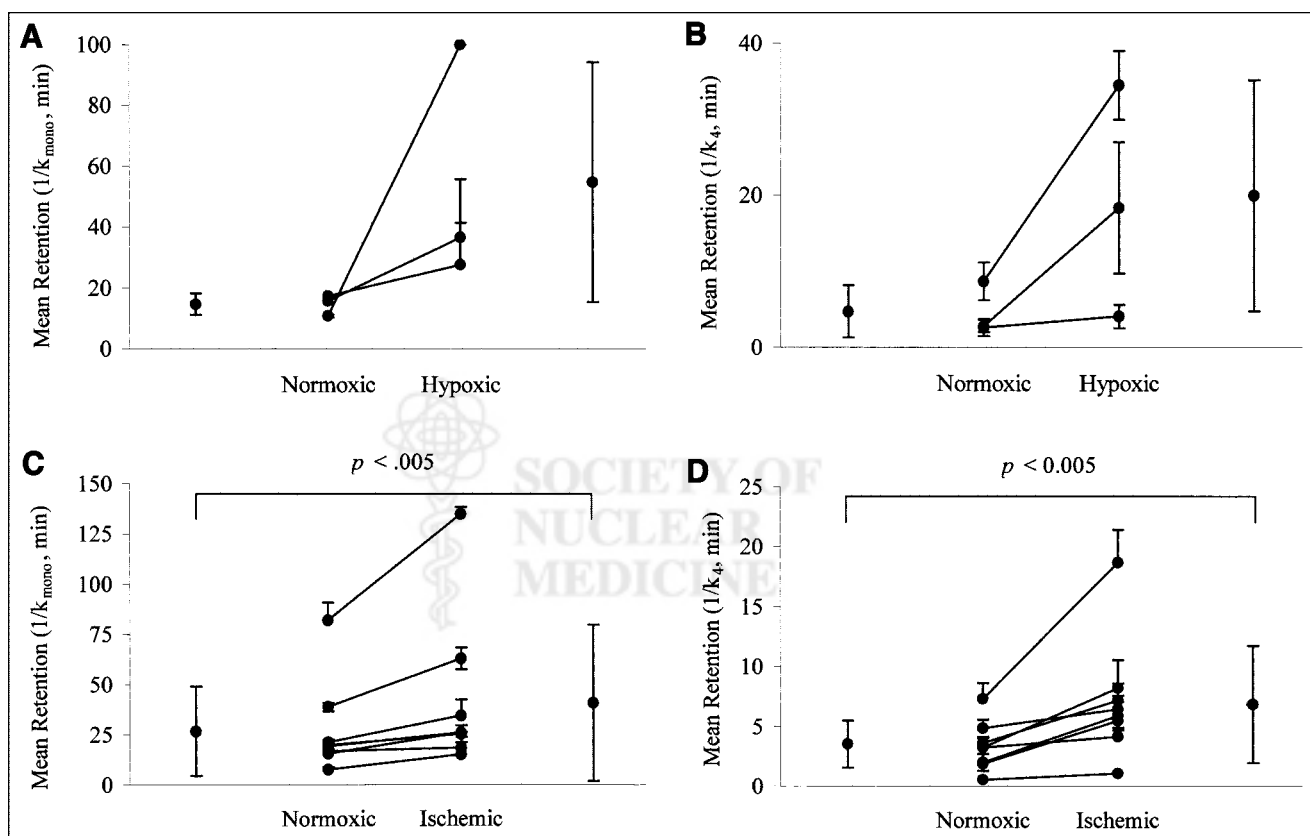


FIGURE 4. Graphs show results for monoexponential analysis of $^*\text{Cu}\text{-ATSM}$ PET (protocol I) (A), kinetic modeling analysis of $^*\text{Cu}\text{-ATSM}$ (protocol I) (B), monoexponential analysis after injection of $^*\text{Cu}\text{-ATSM}$ (protocol II at 3 h) (C), and kinetic modeling analysis after injection of $^*\text{Cu}\text{-ATSM}$ (protocol II at 3 h) (D). Global hypoxia increased tracer retention (B). In each animal, LAD occlusion significantly decreased MBF and concomitantly increased tracer retention. Individual (joined points) and mean values for all animals (far right and far left) of myocardial retention of $^*\text{Cu}\text{-ATSM}$ are given. SD error bars associated with each animal are on individual points; if not seen, bars are within symbol.

TABLE 2
 MBF Determined by $^{15}\text{O}\text{-H}_2\text{O}$ PET and $^*\text{Cu}\text{-ATSM}$ Retention 3 Hours After Coil Placement as Shown by Monoexponential Analysis ($1/k_{\text{mono}}$) and Kinetic Modeling ($1/k_4$) for Protocol II

Dog no.	NLR ($\text{mL} \cdot \text{min}^{-1} \cdot \text{g}^{-1}$)	LADR ($\text{mL} \cdot \text{min}^{-1} \cdot \text{g}^{-1}$)	Flow ratio	Mean retention			
				NLR		LADR	
				$1/k_{\text{mono}}$ (min)	$1/k_4$ (min)	$1/k_{\text{mono}}$ (min)	$1/k_4$ (min)
4	0.57 ± 0.06	0.12 ± 0.01	0.21	38.76 ± 2.10	2.00 ± 0.72	62.89 ± 5.54	5.88 ± 1.18
5	0.48 ± 0.14	0.13 ± 0.02	0.27	19.27 ± 1.19	1.85 ± 0.99	25.97 ± 4.52	5.49 ± 1.51
6	0.45 ± 0.09	0.17 ± 0.03	0.38	19.92 ± 1.71	4.84 ± 0.72	25.13 ± 0.69	6.45 ± 1.11
7	0.32 ± 0.04	0.09 ± 0.03	0.28	81.97 ± 8.73	3.24 ± 0.77	135.10 ± 3.29	8.23 ± 2.30
8	0.39 ± 0.02	0.02 ± 0.04	0.05	21.28 ± 1.36	3.60 ± 0.50	34.48 ± 7.73	7.19 ± 1.40
9	0.73 ± 0.06	0.23 ± 0.12	0.31	15.50 ± 1.11	0.53 ± 0.09	26.11 ± 3.27	1.09 ± 0.54
10	0.92 ± 0.07	0.77 ± 0.15	0.83	19.05 ± 2.90	4.08 ± 0.32	23.36 ± 3.66	5.41 ± 0.38
11	0.60 ± 0.04	0.60 ± 0.05	1.00	16.84 ± 1.08	4.17 ± 0.22	18.28 ± 2.87	3.23 ± 0.71
12	0.76 ± 0.08	0.44 ± 0.07	0.58	7.58 ± 1.30	7.30 ± 1.32	15.15 ± 8.49	18.69 ± 2.73
Mean \pm SD	0.52 ± 0.19	0.28 ± 0.26	$0.48 \pm 0.27^*$	26.69 ± 22.29	3.51 ± 1.97	$40.72 \pm 39.00^*$	$6.85 \pm 4.90^*$

* $P < 0.005$ ischemic vs. baseline. Dogs 9–12 survived > 24 h.

jects, after validation in humans. This validation would include examination during different interventions and a full analysis of metabolites.

Protocol I: Myocardial Retention of $^*\text{Cu}\text{-ATSM}$ in Hypoxic Myocardium

In protocol I, baseline MBF increased approximately 7-fold under hypoxic conditions (Table 1). The variation in MBF at baseline levels was due to the hemodynamic response (and subsequent rate–pressure product) of the animals to the intervention. When the correlation between rate–pressure product and perfusion was determined, a value of $r = 0.94$ ($P < 0.005$) was observed. The retention data demonstrated a significant increase in myocardial tracer retention in the presence of global hypoxia when compared with normoxia on an individual-dog basis, despite the 7-fold increase in MBF (Fig. 4A; Table 1). When the kinetic model was applied, a similar pattern was observed (Fig. 4B; Table 1). The spread in the levels of retention under induced hypoxia correlated directly with the levels of hypoxia obtained in each dog (arterial pO_2 levels decreased to between 35% and 45% of baseline levels).

Protocol II: $^*\text{Cu}\text{-ATSM}$ Retention in Acutely Ischemic Myocardium

In protocol II, 3 h after occlusion, the average MBF at the time of imaging was significantly lower in ischemic regions (LADRs) than in NLRs (Table 2). The variation in MBF at baseline levels was due to the hemodynamic response (and subsequent rate–pressure product) of the animals to the intervention. Of the 4 dogs studied at both 3 h and 24 h after occlusion, all demonstrated variations in the size of the infarcted regions by TTC staining, with a range of MBF values.

Representative PET images obtained over the first 12 min after injection of $^*\text{Cu}\text{-ATSM}$ in an LAD-occluded dog are given in Figure 5A. A graphic summary of the retention data

at 3 h is shown in Figures 4C and 4D. In the dogs studied within 3 h after LAD occlusion, an overall significant increase in myocardial retention in the LADRs, compared with the normal regions ($1/k_{\text{mono}}$, 40.72 ± 39.0 min vs. 26.7 ± 22.3 min, $P < 0.05$), was noted (Fig. 4C). A similar pattern was obtained from kinetic modeling: Retention increased significantly in the LADRs, compared with the NLRs ($1/k_4$, 6.85 ± 4.90 min vs. 3.51 ± 1.97 min, $P < 0.05$) (Fig. 4D). These results are consistent with the presence of hypoxia in the ischemic myocardium.

Of the 4 dogs that were studied at both 3 h and 24 h after occlusion, dogs 9 and 12 had the largest infarcts and dogs 10 and 11 had relatively smaller regions of infarction. In all 4 dogs, an anteroapical ischemic insult and regions of necrosis were demonstrated by analysis of flow patterns at 3 and 24 h, by postmortem positive TTC tissue staining and electronic autoradiography, and by PET imaging (Figs. 5A and 6A). For example, Figure 6A demonstrates an area of significant necrosis but also a surrounding area of increased $^{64}\text{Cu}\text{-ATSM}$ accumulation indicative of a hypoxic zone surrounding the necrotic region. In general, when there was predominately myocardial necrosis at 24 h, there was no significant enhancement in retention of copper-ATSM in necrotic tissue, compared with normal tissue (Fig. 6D). Close examination of $^*\text{Cu}\text{-ATSM}$ myocardial retention patterns showed that, in dogs with small infarcts, retention had not increased 3 h after LAD occlusion, suggesting incomplete coronary occlusion and intermittent ischemia, whereas a significant increase in tracer retention was seen in animals with decreased MBF in the LADRs (dogs 9 and 12) (Figs. 6B and 6D). In these animals, a more pronounced increase in retention was obtained from kinetic modeling than from simple monoexponential analysis (Fig. 6D vs. Fig. 6C). At 24 h, MBF in the LADRs was severely reduced in 3 of the 4 animals (Fig. 6B). However, the patterns of myocardial

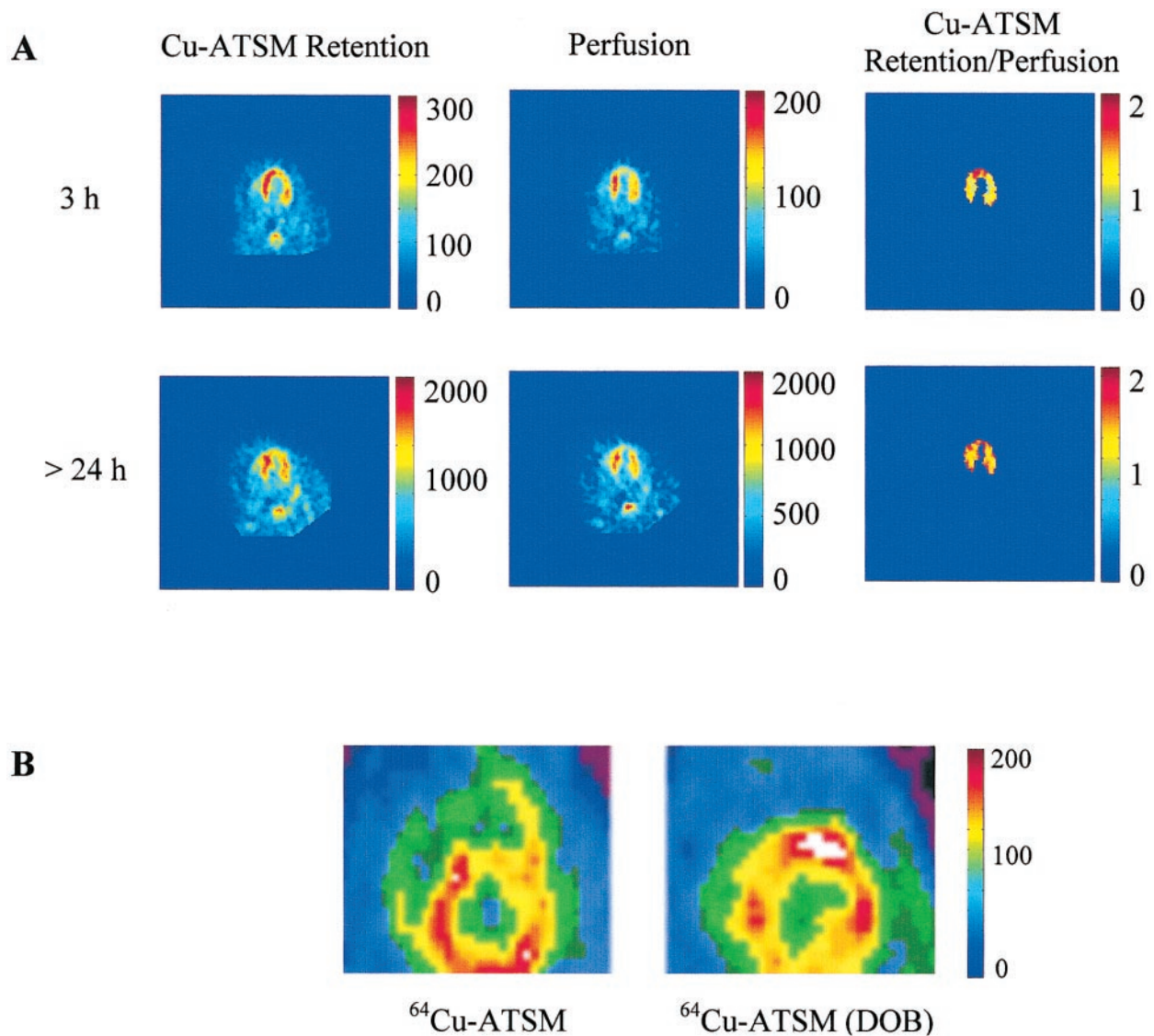


FIGURE 5. (A) Reconstructed midventricular functional PET images after LAD occlusion at 3 and 24 h (protocol II). Top 3 images were obtained after first $^{64}\text{Cu-ATSM}$ injection, 3 h after coronary occlusion, and bottom 3 were obtained after second injection, 24 h later. Horizontal long-axis view is shown, with septum on left, apex on top, and lateral free wall on right. Uptake of tracer is reduced in apical region at both 3 h and 24 h after LAD occlusion, indicating sustained hypoperfusion (perfusion image counts per pixel per minute). In contrast, retention of $^{64}\text{Cu-ATSM}$ (counts per pixel per minute) in apex is higher at 3 h after occlusion than at 24 h. This increase in retention at 3 h can clearly be seen after tracer retention is normalized to tracer uptake ($^{64}\text{Cu-ATSM}$ retention/perfusion [no units]), indicating hypoxic but viable tissue. No increase in retention is observed 24 h after normalization. Absence of $^{64}\text{Cu-ATSM}$ retention in this region 24 h after occlusion is consistent with necrosis, as was confirmed through postmortem TTC staining of heart. (B) Reconstructed midventricular short-axis functional PET images (counts per pixel per minute) show myocardial tracer activity after bolus injection of $^{64}\text{Cu-ATSM}$ (protocol III). Under resting conditions, tracer activity in anterior region is diminished, consistent with hypoperfused but normoxic myocardium. In contrast, during DOB, anterior myocardium shows increased tracer activity despite diminished perfusion to this region, suggesting hypoxia.

retention at 24 h were very different from those observed at 3 h and varied depending on the method of analysis used. The retention values obtained from kinetic modeling showed that animals with severely reduced MBF at 24 h had no increase in retention in the LADR, compared with the NLR. This pattern was consistent with the presence of necrotic tissue and infarct size observed in postmortem staining. The 24-h data therefore confirm that $^{64}\text{Cu-ATSM}$ is not taken up into necrotic regions of the myocardium.

The 3-h protocol has demonstrated $^{64}\text{Cu-ATSM}$ imaging characteristics suitable for acute ischemic syndromes (i.e., acute myocardial infarction) when the flow is limited. For accurate assessment in a clinical situation, a flow tracer would be required to fully evaluate the kinetics of $^{64}\text{Cu-ATSM}$. The 24-h data have demonstrated that $^{64}\text{Cu-ATSM}$ is not retained in necrotic tissue but only in viable hypoxic tissue, with further confirmation from the kinetic modeling that retention is not perfusion related.

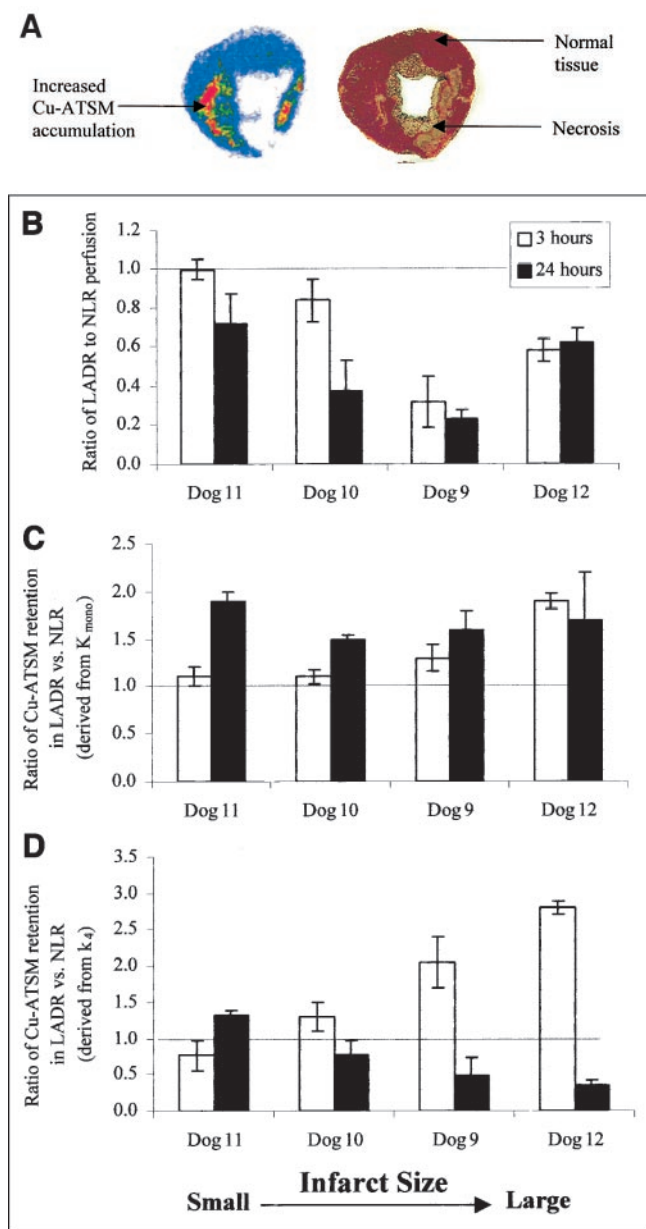


FIGURE 6. (A) On right, TTC-stained 0.5-cm section of myocardium 24 h after occlusion shows significant necrosis. On left, electronic autoradiography shows absence of ^{64}Cu -ATSM retention in this region 24 h after occlusion, consistent with necrosis. Autoradiograph also shows area of increased ^{64}Cu -ATSM accumulation bordering necrotic regions, indicating hypoxic zone surrounding necrotic zone. (B–D) Graphs show MBF (B), $1/k_{\text{mono}}$ retention (C), and $1/k_4$ retention (D) as ratios of LADR to NLR at 3 and 24 h. (C and D) ^{64}Cu -ATSM myocardial retention patterns reveal that tracer retention did not increase 3 h after LAD occlusion in dogs with small infarcts but increased significantly in dogs with decreased MBF in LADRs. At 24 h, MBF in LADRs was severely reduced in 3 of 4 animals (B). Retention values obtained from kinetic modeling (D) show that, in animals with severely reduced MBF at 24 h, retention in LADR decreased. Conversely, retention increased in the only animal (dog 11) in which MBF remained within 80% of normal. This pattern is consistent with necrotic tissue and with infarct size observed through postmortem staining. These data also demonstrate that retention and clearance of ^{64}Cu -ATSM are not related to perfusion.

Protocol III: ^{64}Cu -ATSM Retention After Induction of Demand Ischemia

This protocol closely examined retention of ^{64}Cu -ATSM after induced ischemia without severe flow limitation, which is the most common diagnostic situation in which myocardial hypoxia is documented. In protocol III, MBF was higher in the NLR than in the LADR, indicating reduced perfusion to the LADR (Table 3). Under resting conditions, the transmural MBF between the NLR and LADR and the endocardium-to-epicardium ratios are not significantly different, showing that ischemia was not likely to have been induced with the stenosis. Because we could not confirm this, we assumed that the tissue was under normal levels of oxygenation. During DOB infusion, the transmural MBF increased equivalently in both the NLR and the LADR, while the endocardium-to-epicardium ratio was significantly lower, consistent with the greater flow limitations of the endocardium.

Examples of the time-activity curves, a graphic summary of the monoexponential and modeling data obtained with this protocol, and myocardial PET images generated after injection of ^{64}Cu -ATSM are given in Figures 7A and 7B, Figures 7C–7E, and Figure 5B, respectively. In all 4 dogs, DOB infusion resulted in increased MBF (Table 3) (with a decreasing endocardium-to-epicardium ratio) and a concomitant increase (significant in each dog, $P < 0.005$) in tracer retention in the LADR, compared with the NLR. The kinetic modeling further validated the data from the previous protocols showing that retention of the tracer was not perfusion related.

DISCUSSION

Using canine models of ischemic and hypoxic myocardium and PET, we undertook this study to investigate the potential utility of ^{64}Cu -ATSM for the rapid, noninvasive delineation of hypoxia in myocardium. Hypoxia and ischemia are 2 different physiologic states, and this study was undertaken to examine the oxygen-deprived myocardial states of both hypoxia and ischemia. The protocols in this study clearly demonstrated the usefulness and limitations of ^{64}Cu -ATSM PET for delineating hypoxic myocardial tissue. The data from protocol I resolved the effect of flow on washout and retention of the tracer and confirmed that ^{64}Cu -ATSM can be an effective tracer in the detection of global hypoxia. Protocol II demonstrated the usefulness of ^{64}Cu -ATSM PET for acute ischemic syndromes such as myocardial infarction when flow is limited. The data further demonstrated that ^{64}Cu -ATSM was not retained in necrotic tissue—a finding that has direct clinical implications if one is considering reperfusion therapies. Protocol III demonstrated the hypoxia imaging characteristics of ^{64}Cu -ATSM when ischemia is induced without a severe flow limitation. In this clinically relevant situation, the availability of short-lived isotopes (^{60}Cu and ^{62}Cu) makes repeated imaging sessions a reasonable possibility: For example, a patient could be scanned under resting conditions and then under

TABLE 3
MBF Determined by ⁸⁵Sr (at Rest) and ⁴⁶Sc (with Dobutamine) Microspheres for Protocol III

Dog no.	Region	Rest flow (mL · min ⁻¹ · g ⁻¹)	DOB flow (mL · min ⁻¹ · g ⁻¹)	Flow ratio	Ratio*	
					Rest	DOB
13	NLR	0.83 ± 0.31	1.73 ± 0.52	2.12	0.92	0.82
	LADR	0.31 ± 0.21 [†]	0.73 ± 0.47 [†]	2.35	0.89	0.22
14	NLR	1.11 ± 0.18	2.23 ± 0.32	2.01	1.16	0.99
	LADR	0.63 ± 0.32 [†]	1.37 ± 0.24 [†]	2.18	0.98	0.45
15	NLR	0.67 ± 0.09	1.93 ± 0.34	2.88	0.94	1.03
	LADR	0.52 ± 0.06 [†]	1.29 ± 0.32 [†]	2.48	1.01	0.44
16	NLR	0.78 ± 0.06	1.73 ± 0.34	2.22	0.97	0.98
	LADR	0.63 ± 0.18 [†]	0.94 ± 0.34 [†]	1.49	0.84	0.32
Mean ± SD	NLR	0.85 ± 0.19	1.91 ± 0.24	2.31 ± 0.39	1.00 ± 0.11	0.96 ± 0.36
Mean ± SD	LADR	0.52 ± 0.15 [‡]	1.17 ± 0.44 [‡]	2.13 ± 0.44	0.93 ± 0.08	0.36 ± 0.11 [‡]

*Ratio of microsphere-determined flow between endocardium and epicardium.

[†]*P* < 0.05 LADR vs. NLR.

[‡]*P* < 0.05 LADR vs. NLR.

DOB stress. Results from kinetic modeling demonstrated that this may be a more powerful tool in delineating myocardial hypoxia than is simple monoexponential analysis. The results demonstrated the different retention kinetics of *Cu-ATSM in viable, hypoxic, and necrotic tissues and confirmed that retention of *Cu-ATSM is not perfusion related. However, although this model has initially been shown to be better than monoexponential analysis, the 2-compartment model was used for feasibility purposes and requires further validation before full implementation.

Tissue hypoxia plays a central role in the pathogenesis of myocardial ischemia. The other manifestations of myocardial ischemia, including perturbations in metabolism, mechanical dysfunction, and electric instability, are secondary to hypoxia. Currently, methods of diagnosing myocardial ischemia include those such as coronary angiography, which detect abnormalities in MBF; those such as stress electrocardiography and echocardiography, which detect the secondary manifestations of ischemia; and those such as the multiple imaging methods that measure myocardial perfusion. Unfortunately, a direct correlation does not always exist between the readouts from these imaging techniques and the presence of myocardial ischemia. For example, the presence of coronary artery stenosis does not always imply abnormalities in myocardial perfusion. Moreover, the presence of reversible perfusion abnormalities on rest/stress myocardial perfusion imaging may signify impairment in myocardial vasodilatory reserve but not necessarily inadequate oxygen supply to meet demand and, thus, myocardial ischemia. Conversely, in the presence of resting electrocardiographic abnormalities or systolic dysfunction, it frequently is difficult to definitively couple the presence of these abnormalities with the induction of myocardial ischemia. Consequently, accurate detection of myocardial hypoxia would have numerous applications both in cardiovascular research and in the management of patients with

cardiovascular disease. The detection of hypoxia in these patients could potentially further our understanding of these cardiac disease processes as well as provide an important marker to monitor the efficacy of novel strategies to treat them. Given the importance of the presence of myocardial ischemia and, thus, hypoxia as a marker of increased cardiac risk in patients with coronary artery disease, hypoxic imaging may prove useful in assigning prognosis in patients with this disease. The results of the current study suggest that PET with *Cu-ATSM may potentially be useful in the detection of hypoxia both after acute coronary occlusion and during the demand-induced ischemia that occurs with stress testing. Certain characteristics are desirable in an imaging agent for myocardial hypoxia. First, retention of the agent should be directly proportional to the decline in tissue oxygenation. Second, the myocardial kinetics of the agent should permit rapid imaging and relatively simple image interpretation. Finally, the imaging approach should be available for clinical use. To a large extent, PET imaging with *Cu-ATSM fulfills these requirements. In isolated perfused hearts, retention of *Cu-ATSM is directly proportional to tissue oxygenation (16,17). Imaging can be completed within 20–45 min after tracer administration, and measurement of the myocardial retention rate of copper-ATSM is straightforward. The kinetics of *Cu-ATSM are such that administration of DOB and *Cu-ATSM could occur out of the PET scanner and then images such as that shown in Figure 5B (right) can be obtained after the patient is subsequently positioned in the scanner. The continued wide dissemination of PET, primarily because of its oncologic applications, and the ability to radiolabel ATSM with positron-emitting radionuclides of copper increase the potential availability of this imaging method.

The positron-emitting isotopes of copper—⁶⁰Cu, ⁶¹Cu, and ⁶⁴Cu—can be produced at high specific activity on all biomedical cyclotrons using identical target systems and

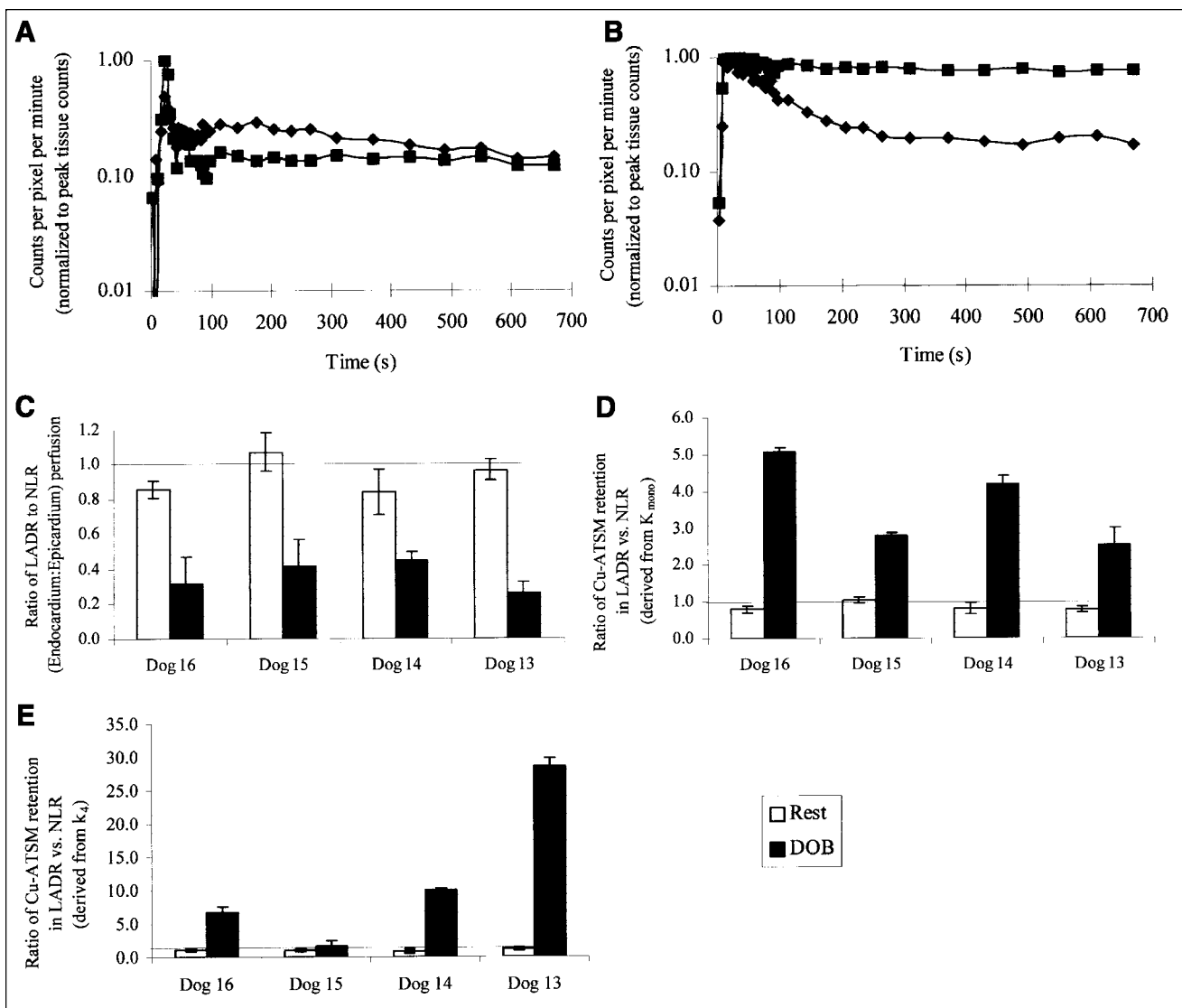


FIGURE 7. (A) In myocardial time-activity curves obtained after injection of ^{64}Cu -ATSM in dog 13 at rest (protocol III), normal septal/lateral region (\blacklozenge) and apical region (\blacksquare) show similar kinetics. Although data collection continued until 45 min, figure shows only first 12 min, for clarity. (B) In myocardial time-activity curves obtained after injection of ^{64}Cu -ATSM in dog 13 after DOB infusion (protocol III), normal septal/lateral region (\blacklozenge) shows rapid washout kinetics but apical region (\blacksquare) shows uptake and excellent tracer retention, indicating hypoxia. Although data collection continued until 45 min, figure shows only first 12 min, for clarity. (C-E) Graph of MBF (ratio of LADR to NLR [endocardium to epicardium]) (C) and graphs of $1/k_{\text{mono}}$ retention (D) and $1/k_4$ retention (E) expressed as ratios between LADR and NLR at rest and stress show myocardial retention of ^{64}Cu -ATSM for each dog in protocol III. In all cases, DOB infusion significantly increased tracer retention in damaged apical regions ($P < 0.005$), despite increase in MBF (Table 3).

chemistry (20,21). The technology for the production of ^{64}Cu , ^{61}Cu , and ^{60}Cu (Newton Scientific, Inc., Cambridge, MA) has been obtained by institutions in the United States, Europe, Japan, and Canada. As shown in the current study, the resolution qualities of these copper radioisotopes (taking the 2 extremes, ^{64}Cu and ^{60}Cu) are similar in good-quality PET cameras. The distance traveled by the positron before annihilation, or the positron range, will cause additional blurring that prevents the discrimination of small structures. An understanding of the positron range spectra for each isotope comes from a detailed analysis of their respective

decay schemes. In β^+ decay, the positron will be emitted with a spectra that can be defined by a Fermi function, with the endpoint determined by the Q-value of the decay. ^{64}Cu decays by positron emission, with a branching ratio of 17.4% and a maximum β^+ energy of 653 keV. This endpoint energy is thus similar to that of ^{18}F decay (634 keV) (31), and the maximum range of the positron will therefore be similar to that of ^{18}F , with an average value of 0.4 mm in water. Although the Q-value of the β^+ decay of ^{60}Cu is high (5.105 MeV), the decay will proceed to excited states in ^{60}Ni . The most probable levels are 1.3325 MeV (5%), 2.159

MeV (15%), 3.124 MeV (49%), and 3.194 MeV (11.6%) (31). The maximum energy of the β^+ will therefore be strongly reduced. The maximum positron range of such high-energy positrons is close to 16 mm in water. However, these are relatively rare events, and on average, the positron range will be approximately only 3 mm in water. The imaging performance of ^{60}Cu was therefore only slightly impaired relative to ^{64}Cu , and in particular, the long-range component of the ^{60}Cu β^+ spectra reduced the contrast only around small structures, as is apparent on the ^{60}Cu phantom of Derenzo et al. (23), in which the smallest rods (2.5 mm) could not be identified. The complex decay scheme of ^{60}Cu will also result in the emission of numerous γ -rays with energy mostly greater than 0.826 MeV. These γ -rays detected in coincidence with annihilation photons will contribute to reducing camera performance. These events will increase camera dead time and create a uniform distribution of counts in the images. Given the relatively weak activity in the field of view, the number of prompt γ -rays associated with the decay of ^{60}Cu did not reduce image quality in comparison with image quality from the ^{64}Cu phantom.

The easy and economic production of a sterile and radiochemically pure preparation of ^{60}Cu -ATSM at Washington University School of Medicine takes approximately 50 min. Between February 1998 and April 2002, 92 patients with a variety of tumors, including those of the head and neck, lung, and cervix, were imaged with ^{60}Cu -ATSM in ongoing clinical trials (21,32,33). ^{61}Cu , with its 3.32-h half-life, can feasibly be produced and supplied by national distribution centers, just as are ^{18}F -radiopharmaceuticals (21). The longer-lived ^{64}Cu is currently produced and supplied through a National Institutes of Health/National Cancer Institute-funded research resource grant to more than 15 institutions throughout the United States (34). Preparation of ^{62}Cu through a $^{62}\text{Zn}/^{62}\text{Cu}$ generator has been reported by several groups (13,22,35,36), and one such system has been commercialized (22). The wide dissemination of the copper radionuclides, and the availability of shorter-lived isotopes that allow for repeated imaging, makes the use of copper radiopharmaceuticals particularly attractive.

One aim of this study was to investigate whether mathematic modeling of the kinetics of ^{60}Cu -ATSM, compared with simple clearance analysis of myocardial ^{60}Cu -ATSM curves, results in more accurate and reliable detection of hypoxia. Myocardial clearance analysis is simple and requires only the washout phase of the myocardial curves. In contrast, defining the entire myocardial kinetic of ^{60}Cu -ATSM using kinetic modeling requires ^{60}Cu -ATSM myocardial as well as blood activity over the entire study period. To ensure that blood activity is not contaminated by labeled metabolites, it must be corrected for these metabolites, and such correction requires blood sampling and analysis. It is hoped that a single multiexponential function will be clinically applicable after validation in humans, including validation during different interventions and a full analysis of metabolites.

Global myocardial hypoxia without ischemia (protocol I) was detected as well by monoexponential clearance analysis as by kinetic modeling; both methods demonstrated a 4-fold increase in retention. Furthermore, regional variations of $1/k_{\text{mono}}$ and $1/k_4$ values were also comparable ($23\% \pm 26\%$ vs. $30\% \pm 11\%$, $P =$ not statistically significant). Both methods are also similar in their ability to assess myocardial hypoxia in the presence of ischemia (protocol II, 3 h, and protocol III). Regional variations of $1/k_{\text{mono}}$ retention tended to be lower than those of $1/k_4$ retention ($13\% \pm 12\%$ vs. $22\% \pm 13\%$, $P = 0.09$). However, in the 4 animals studied 24 h after LAD occlusion (protocol III), and in which hypoxia as well as necrosis was present, retention values derived from monoexponential clearance were different from those derived from kinetic modeling (Fig. 6C vs. Fig. 6D). Monoexponential clearance analysis showed a consistent and significant increase in retention in all 4 animals, suggesting the presence of hypoxia but not of necrosis. These results were inconsistent with the postmortem TTC staining results. In contrast, kinetic modeling analysis demonstrated similar or a lowering of retention in the LADR, compared with the NLRs, in the 3 animals that had sustained severe ischemia and an MBF of less than 50% of normal. However, an increase in retention was shown in the ischemic regions of the only animal in which perfusion to the LADRs was within 80% of normal. Thus, differences in retention between hypoxic and necrotic tissue were detected with kinetic modeling but not with monoexponential analysis. This discrepancy is understandable when one considers that kinetic modeling takes into account spillover effects and partial-volume corrections and uses the true input function. Further, kinetic modeling decouples perfusion kinetics from retention and washout of the tracer; the insensitive nature of the monoexponential analysis is inadequate for this particular analysis. These results strongly suggest that kinetic modeling will better detect hypoxia in ischemic myocardium. Although this model is superior to monoexponential analysis, the 2-compartment model in the current study was used for feasibility purposes and requires further validation before full implementation.

^{123}I and $^{99\text{m}}\text{Tc}$ -misonidazole analogs have been investigated as hypoxia-avid agents for use with SPECT (2). The $^{99\text{m}}\text{Tc}$ -compounds, $^{99\text{m}}\text{Tc}$ -HL91, BMS-181321, and BMS-194796, have demonstrated increased uptake in hypoxic and low-flow ischemic myocardium (5–7,37). BMS-181321 displayed high liver uptake, which excluded this tracer from routine clinical use, but the analog BMS-194796 may provide a realistic alternative, with reduced hepatic uptake and increased tracer uptake in ischemic tissue (38). $^{99\text{m}}\text{Tc}$ -HL91 is one of the most promising $^{99\text{m}}\text{Tc}$ -agents for both the imaging of tumor hypoxia (39) and the imaging of ischemic myocardium (5); however, acutely injured nonviable myocardium has shown $^{99\text{m}}\text{Tc}$ -HL91 uptake and retention similar to those of normal myocardium (40). In PET imaging with ^{18}F -FMISO after 3 h of coronary occlusion in dogs, Shelton et al. showed that the residual fraction of activity

averaged $23\% \pm 18\%$ in ischemic myocardium, compared with $2\% \pm 1\%$ in normal tissue (10). A similar study found that the binding ratio of ^{18}F -FMISO at 4 h was 1.8–2.4 times higher in ischemic regions than in normal regions (11). In the present study, ^{64}Cu -ATSM was taken up rapidly and selectively in hypoxic and ischemic tissue within 20 min after administration, showing that differences between hypoxic and normal tissue can be imaged. Our data, by showing that ^{64}Cu -ATSM was not retained in necrotic tissue (protocol II, 24 h), confirmed that ^{64}Cu -ATSM is an efficient tracer for the delineation of myocardial hypoxia.

CONCLUSION

ATSM PET (labeled with the positron-emitting isotopes of copper) offers a viable alternative to the reported SPECT hypoxia agents and the PET agent ^{18}F -FMISO. Its economic and rapid production makes this tracer attractive for PET imaging, with repeated imaging sessions using the short-lived copper isotopes being a reasonable possibility. ^{64}Cu -ATSM kinetics were shown to be independent of flow and to be particularly effective for delineating hypoxia in clinically relevant acute coronary syndromes and in demand-induced ischemia. The encouraging results from this protocol have led us to undertake a pilot clinical study at our institution, where we are testing the feasibility of PET using this tracer to detect myocardial hypoxia resulting from inducible myocardial ischemia in patients with newly diagnosed or known coronary artery disease.

ACKNOWLEDGMENTS

The authors thank Mark Nolte, Margaret Morris, and Nicole Mercer for technical assistance with the animal studies; Dr. Deborah McCarthy, Thomas F. Voller, and Todd A. Perkins for assistance with production of the copper radionuclides; and Dr. Douglas Rowland, Linda M. Becker, and Dr. Joon Young Kim for expert assistance with the PET imaging. This study was supported by grant 2-PO1-HL-13851 from the National Institutes of Health.

REFERENCES

- Chapman JD, Zanzonico P, Ling CC. On measuring hypoxia in individual tumors with radiolabeled agents. *J Nucl Med.* 2001;42:1653–1655.
- Nunn A, Linder K, Strauss HW. Nitroimidazoles and imaging hypoxia. *Eur J Nucl Med.* 1995;22:265–280.
- Parliament MB, Chapman JD, Urtasun RC. Non-invasive assessment of human tumour hypoxia with ^{125}I -iodoazomycin arabinoside: preliminary report of a clinical study. *Br J Cancer.* 1992;65:90–95.
- Grosher D, McEwan AJB, Parliament MB, et al. Imaging tumor hypoxia and tumor perfusion. *J Nucl Med.* 1993;34:885–888.
- Okada RD, Johnson G, Nguyen KN, et al. "Hot spot" detection of ischemic myocardium in vivo by gamma camera imaging. *Circulation.* 1998;97:2557–2566.
- Ng CK, Sinusas AJ, Zaret B, Souter R. Kinetic analysis of technetium-99m-labeled nitroimidazole (BMS181321) as a tracer of myocardial hypoxia. *Circulation.* 1995;92:1261–1268.
- Wedeking P, Yost F, Wen M, et al. Comparison of the biological activity of the isomers of the Tc-99m-nitroimidazole complex BMS-194796 [abstract]. *J Nucl Med.* 1995;36(suppl):17P.
- Shelton ME, Dence C, Hwang D-R, Welch MJ, Bergmann SR. Myocardial

kinetics of fluorine-18 misonidazole: a marker of hypoxic myocardium. *J Nucl Med.* 1989;30:351–358.

- Martin GV, Caldwell JH, Graham MM, et al. Non-invasive detection of hypoxic myocardium using fluorine-18-fluoromisonidazole and positron emission tomography. *J Nucl Med.* 1992;33:2202–2208.
- Shelton ME, Dence CS, Hwang D-R, Herrero P, Welch MJ, Bergmann SR. In vivo delineation of myocardial hypoxia during coronary occlusion using fluorine-18 fluoromisonidazole and positron emission tomography: a potential approach for identification of jeopardized myocardium. *J Am Coll Cardiol.* 1990;16:477–485.
- Martin GV, Caldwell JH, Rasey JS, Grunbaum Z, Cerqueira M, Krohn KA. Enhanced binding of the hypoxic cell marker [^3H]fluoromisonidazole in ischemic myocardium. *J Nucl Med.* 1989;30:194–201.
- Green MA. A potential copper radiopharmaceutical for imaging the heart and brain: copper-labeled pyruvaldehyde bis(N_4 -methylthiosemicarbazone). *Nucl Med Biol.* 1987;14:59–61.
- Green MA, Mathias CJ, Welch MJ, et al. Copper-62-labeled pyruvaldehyde bis(N_4 -methylthiosemicarbazone)copper(II): synthesis and evaluation as a positron emission tomography tracer for cerebral and myocardial perfusion. *J Nucl Med.* 1990;31:1989–1996.
- Lewis JS, McCarthy DW, McCarthy TJ, Fujibayashi Y, Welch MJ. Evaluation of ^{64}Cu -ATSM in vivo and in vitro in a hypoxic tumor model. *J Nucl Med.* 1999;40:177–183.
- Dearling JJJ, Lewis JS, Mullen GED, Welch MJ, Blower MJ. Copper bis(thiosemicarbazone) complexes as hypoxia imaging agents: structure-activity relationships. *J Biol Inorg Chem.* 2002;7:249–259.
- Fujibayashi Y, Taniuchi H, Yonekura Y, Ohtani H, Konishi J, Yokoyama A. Copper-62-ATSM: a new hypoxia imaging agent with high membrane permeability and low redox potential. *J Nucl Med.* 1997;38:1155–1160.
- Fujibayashi Y, Cutler CS, Anderson CJ, et al. Comparative studies of Cu-64-ATSM and C-11-acetate in an acute myocardial infarction model: ex vivo imaging of hypoxia in rats. *Nucl Med Biol.* 1999;26:117–121.
- Lewis JS, Sharp TL, Laforest R, Fujibayashi Y, Welch MJ. Tumor uptake of copper-diacetyl-bis(N_4 -methylthiosemicarbazone): effect of changes in tissue oxygenation. *J Nucl Med.* 2001;42:655–661.
- Takahashi N, Fujibayashi Y, Yonekura Y, et al. Copper-62 ATSM as a hypoxic tracer in myocardial ischemia. *Ann Nucl Med.* 2001;15:293–296.
- McCarthy DW, Shefer RE, Klinkowstein RE, et al. Efficient production of high specific activity ^{64}Cu using a biomedical cyclotron. *Nucl Med Biol.* 1997;24:35–43.
- McCarthy DW, Bass LA, Cutler PD, et al. High purity production and potential applications of copper-60 and copper-61. *Nucl Med Biol.* 1999;26:351–358.
- Haynes NG, Lacy JL, Nayak N, et al. Performance of a $^{62}\text{Zn}/^{62}\text{Cu}$ generator in clinical trials of PET perfusion agent ^{62}Cu -PTSM. *J Nucl Med.* 2000;41:309–314.
- Derenzo SE, Budinger TF, Juesman RH, Cahoon JL, Vuletic T. Imaging properties of a positron tomograph with 280 BGO crystals. *IEEE Trans Nucl Sci.* 1981;NS-28:81–99.
- Bredle DL, Chapler CK, Cain SM. Metabolic and circulatory responses of normoxic skeletal muscle to whole-body hypoxia. *J Appl Physiol.* 1988;65:2063–2068.
- Bergmann SR, Lerch RA, Fox KAA, et al. Temporal dependence of beneficial effects of coronary thrombolysis characterized by positron tomography. *Am J Med.* 1982;73:573–581.
- Fishbein MC, Meerbaum S, Rit J, et al. Early phase acute myocardial infarct size quantification: validation of the triphenyl tetrazolium chloride tissue enzyme staining technique. *Am Heart J.* 1981;101:593–600.
- Kloner RA, Darsee JR, DeBoer LWV, Carlson N. Early pathologic detection of acute myocardial infarction. *Arch Pathol Lab Med.* 1981;105:403–406.
- Knabb RM, Fox KAA, Sobel BE, Bergmann SR. Characterization of the functional significance of subcritical coronary stenosis with H_2^{15}O and positron emission tomography. *Circulation.* 1985;71:1271–1278.
- Herrero P, Markham J, Weinheimer CJ, et al. Quantification of regional myocardial perfusion with generator-produced ^{62}Cu -PTSM and positron emission tomography. *Circulation.* 1993;87:173–183.
- Herrero P, Markham J, Bergmann SR. Quantitation of myocardial blood flow with H_2^{15}O and positron emission tomography: assessment and error analysis of a mathematical approach. *J Comput Assist Tomogr.* 1989;13:862–873.
- National Nuclear Data Center, Brookhaven National Laboratory. Nuclear decay data in the MIRD format. Available at: <http://www.nndc.bnl.gov/nndc/formmird.html>. Accessed August 22, 2002.
- Chao C, Bosch WR, Mutic S, et al. A novel approach to overcome hypoxic tumor resistance: Cu-ATSM-guided intensity-modulated radiation therapy. *Int J Radiat Biol Phys.* 2001;49:1171–1182.

33. Dehdashti F, Mintun MA, Lewis JS, Govindan R, Welch MJ. Evaluation of tumor hypoxia with Cu-60-ATSM and PET [abstract]. *J Nucl Med.* 2000;41(suppl):34P.
34. McCarthy DW, Bigott HM, Perkins TA, Voller TF, Welch MJ. A research resource in radionuclide research. *J Labelled Compds Radiopharm.* 2001;44: S817–S819.
35. Fujibayashi Y, Matsumoto K, Yonekura Y, Konishi J, Yokoyama A. A new zinc-62/copper-62 generator as a copper-62 source for PET radiopharmaceuticals. *J Nucl Med.* 1989;30:1838–1842.
36. Robinson JGD, Zielinski FW, Lee AW. The zinc-62/copper-62 generator: a convenient source of copper-62 for radiopharmaceuticals. *Int J Appl Radiat Isot.* 1980;31:111–116.
37. Rumsey WL, Patel B, Linder K. Effect of graded hypoxia in retention of technetium-99m-nitroheterocycle in perfused rat hearts. *J Nucl Med.* 1995;36:632–636.
38. Rumsey WL, Patel B, Kuczynski B, et al. Comparison of two novel technetium agents for imaging ischemic myocardium [abstract]. *Circulation.* 1995;92(suppl): I-181.
39. Cook GJR, Houston S, Barrington SF, Fogelman I. Technetium-99m-labeled HL91 to identify tumor hypoxia: correlation with fluorine-18-FDG. *J Nucl Med.* 1998;39:99–103.
40. Okada RD, Johnson G, Nguyen KN, Carlson LR, Beju D. HL-91-technetium-99m: a new marker of viability in ischemic myocardium. *J Nucl Cardiol.* 1999;6:306–315.

